Solar Energy Materials and Solar Cells (2013), 113, 115-122.
DOI: http://dx.doi.org/10.1016/j.solmat.2012.12.012

Toward a quantitative model for suspended particle devices: Optical scattering and absorption coefficients

David Barrios [a,*], Ricardo Vergaz [a], Jose M. Sanchez-Pena [a], Claes G. Granqvist [b], Gunnar A. Niklasson [b]

[a] Grupo de Displays y Aplicaciones Fotonicas, Departamento de Tecnologia Electronica, Universidad Carlos III de Madrid, C/Butarque 15, E-28911 Leganés, Madrid, Spain

[b] Department of Engineering Sciences, The Angström Laboratory, Uppsala University, P.O. Box 534, SE-75121 Uppsala, Sweden

* Corresponding author. Tel.: +34 916248390; fax: +34 916249430. *E-mail address:* dbarrios@ing.uc3m.es (D. Barrios).

Abstract: Suspended particle devices (SPDs) allow rapid voltage-controlled modulation of their optical transmit-tance and are of interest for solar-energy-related and other applications. We investigated the spectral total and diffuse transmittance of an SPD, including its angular dependence. The optical modulation was large for visible light but almost nil in the infrared, and the devices had noticeable haze. A theoretical two-flux model was formulated and provided a quantitative description of the absorption and scattering coefficients and thereby of the detailed optical performance. This analysis gives a benchmark for assessing improvements of the SPD technology as well as for comparing it with alternative technologies for optical modulation.

Keywords: Suspended particle device, Optical properties, Diffuse transmittance and reflectance, Scattering and absorption coefficients, Two-flux theory,

1. Introduction

Electrically modulated optical properties are of interest for numerous applications [1–3], such as for energy efficient and comfort enhancing ''smart windows'' in buildings and vehicles, eyeware including goggles and helmets, anti-dazzling rear-view mirrors for cars and trucks, panels for temperature control of spacecraft, etc. The most important of these applications, seen in a global perspective, is the ''smart windows'' that are significant for reducing the energy used in the built environment [4,5] and hence for CO_2 abatement and for combating global warming. The devices enabling modulation of luminous and solar transmittance can be of several different kinds such as electrochromic five-layer ''battery-type'' devices based on inorganic oxides [6–8], hydrides [9,10] or on organic materials [11]; suspended-particle devices (SPDs) [12–16]; polymer-dispersed liquid crystals [17,18]; and reversible electroplating systems [19,20]. The least investigated and understood of these seems to be the SPDs, which at first sight is surprising since this type of devices has a venerable history and goes back to the ''light valves'' introduced by Edwin Land in the 1930s and forming the basis of a long series of patents [21]. The purpose of this paper is to investigate and model a typical SPD, thereby allowing a better understanding of its functioning, characteristic features, and potential limitations, and hence laying a foundation for academic inquiry into SPDs as a complement to their currently ongoing industrial development.

An SPD consists of a polymer layer, containing a large number of light absorbing and polarizable particles, between two sheets of glass or plastic coated with transparent and electrically conducting thin films facing the polymer layer. The particles should be less than ~200 nm in size in order to avoid excessive haze. They consist of polyiodides or, more generally, polyhalides and exhibit large optical anisotropy. The most well known compound of this class is heraphatite (quinine bisulfate polyiodide) [22], which was extensively used in early work on polarizers and other optical devices [23]. Its optical anisotropy was recently described theoretically in considerable detail [24]. A number of related compounds have been used in later work on SPDs [13,25].

The optical transmittance of the SPDs can be adjusted either automatically, by using a photocell-based feedback or some other control device, or adjusted manually with a rheostat or a remote control by a user. Applying a sufficient electric voltage to the polymer layer, via the transparent conducting films, makes the particles align and become parallel to the field thereby yielding a higher transmittance. Decreasing the voltage makes the window darker until it reaches a bluish-black color. In other words, in the ''off'' state, when no voltage is applied, the particles are randomly dispersed and therefore absorb light and create a dark appearance; conversely, in the ''on'' state the particles align and the character of the glass changes from dark to clear. The functioning principles are shown in the upper two panels in Fig. 1. An intermediate voltage can provide a transmittance lying between

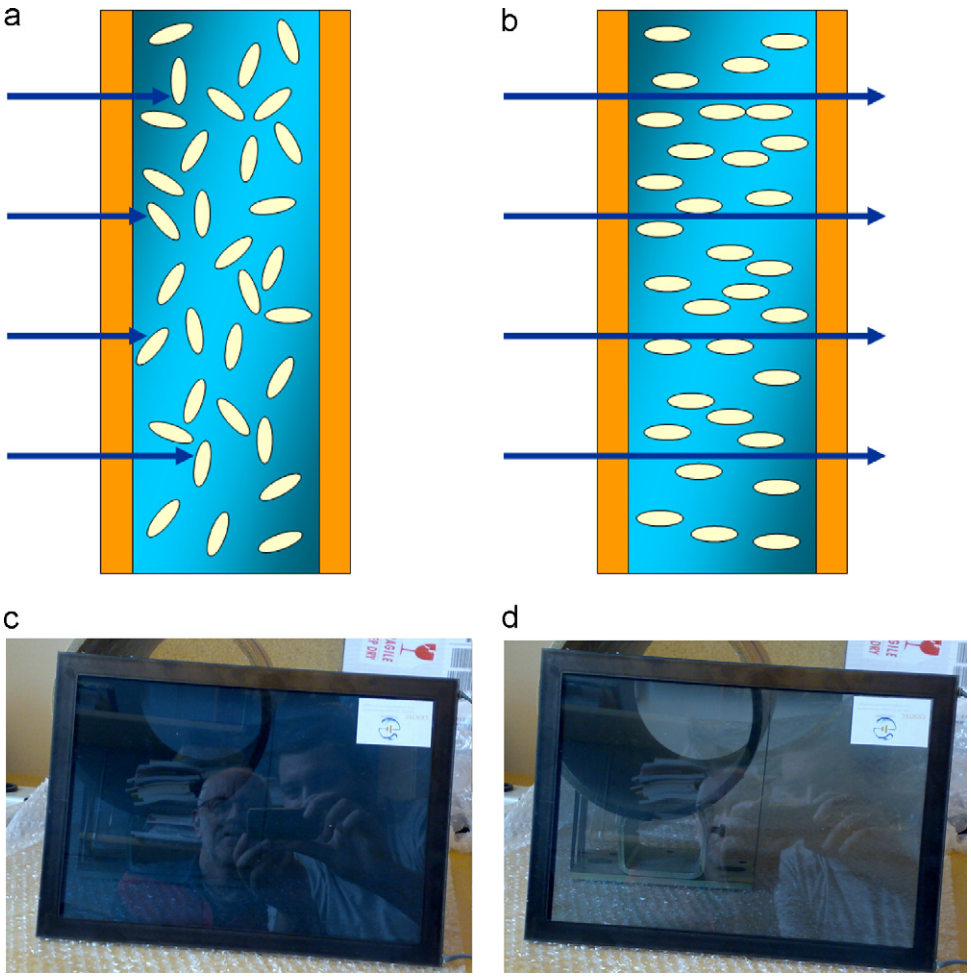

Fig. 1. Upper panels (a) and (b) illustrate the functioning principles of an SPD in "off" and "on" states, respectively, and lower panels (c) and (d) are photographs of the SPD, reported on below, in these two states.

that for the "off" and "on" states. The voltage must be AC in order not to lead to time-dependent degradation of the SPD.

2. Experiments

2.1. Devices

The SPD investigated in this work has an active area of 28×22 cm^2 and a thickness of 300 μm. It is a CriRegulite device supplied by CRICURSA (Cristales Curvados S. A., Barcelona, Spain), which is a licensee of Research Frontiers, Inc. (Woodbury, NY, USA). The optically active layer was made as detailed elsewhere [26] by means of a cross-linked polymer matrix containing droplets comprising a suspension of polyhalide particles. The layer was spread as an emulsion over a 4-mm-thick glass plate pre-coated with a transparent and electrically conducting film of tin-doped indium oxide (In_2O_3:Sn, known as ITO). The refractive indices of the droplets and their surrounding matrix matched to within 0.005, and the droplets were $\sim$1 μm in size. This design leads to a low-scattering and bluish device as apparent in the lower two panels in Fig. 1.

The SPD was operated with a sinusoidal signal at 50 Hz and a peak voltage U between 0 and 100 V. This voltage was obtained by using a function generator in series with a broad-band linear amplifier (FLC Electronic AB, model F10A) with an amplification of 10 times and a maximum input voltage of $\pm$10 V. The electrical current drawn by the transparent SPD was measured with a digital multi-meter (Keithley 197 A).

2.2. Optical measurements

Total reflectance R_{tot} and transmittance T_{tot}, as well as diffuse reflectance R_{diff} and transmittance T_{diff}, were measured in the $300 < \lambda < 2500$ nm wavelength range by use of a double-beam spectrophotometer (Perkin-Elmer Lambda 900) equipped with an integrating sphere. Reflectance and transmittance were recorded at normal incidence with 5 nm resolution, and the diffuse components represented the light that was not specularly reflected or transmitted through the sample, as shown in Fig. 2. In an integrating sphere, light reflected or transmitted by the sample hits the sphere wall and is reflected repeatedly until eventually it is absorbed by the detector. The inside of such a sphere is coated with a white diffuse coating, usually of $BaSO_4$, which is a close approximation to a Lambertian surface that hypothetically scatters 100% of the incident light evenly over the sphere surface. In an actual measurement, losses from absorption by the sphere wall and light escaping through the entrance ports must be corrected for [27,28].

Three scans are needed for samples which scatter transmitted and reflected light, namely (i) a reference scan with a $BaSO_4$ reference plate at the sample port (R in Fig. 2a), (ii) a measurement of the total reflectance or transmittance with the sample positioned at the sample port or entrance port (T in Fig. 2a),

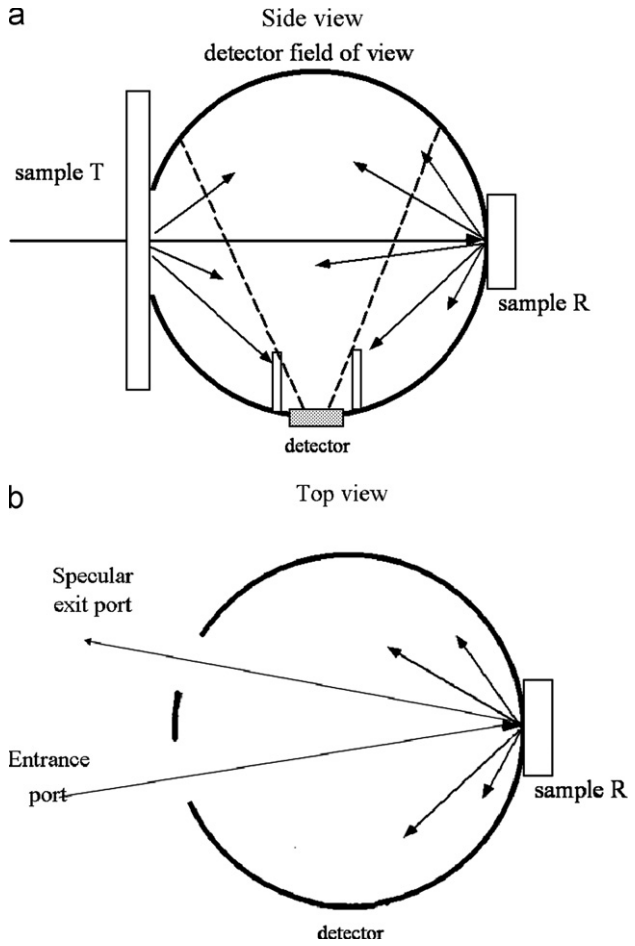

Fig. 2. Schematic view of an integrating sphere used for measuring transmittance *T* and reflectance *R*. Panel (a) shows side view and panel (b) shows top view and illustrates measurement of diffuse reflectance.

respectively, and (iii) a recording for which the specular component is allowed to escape by opening a specular exit port so that the diffuse reflectance (as indicated in Fig. 2b) or transmittance (by putting an absorbing black cone behind the sample *R* port in Fig. 2a) only can be determined. Expressions for reflectance and transmittance are given by ratios between the pertinent recorded signals. Corrections for the reflectance of the reference plate are important for the diffuse components [27,28], but port losses were negligible in our case. Specular and direct components, R_{spec} and T_{dir}, were derived by subtracting the diffuse components R_{diff} and T_{diff} from the total components R_{tot} and T_{tot}.

Complementary recordings of angular-dependent transmittance spectra in the $300 < \lambda < 1100$ nm range were taken with an integrating sphere set-up detailed elsewhere [29]. The off-normal incidence angle θ was set from 0 to 60° with 15° intervals. A quartz crystal polarizer located in front of the experimental assembly was used for obtaining *s* or *p* polarized light. Total transmittance values were calculated as an average of the data obtained with both polarizations.

3. Theory

The optical properties of light scattering media are characterized by the spectrally dependent absorption and scattering coefficients, denoted β and α, respectively, whose sum is the extinction coefficient *E*, i.e., $E=\alpha+\beta$. Determining these coefficients from experimental spectra is a difficult problem. However, the optical properties of a layer exhibiting specular and diffuse reflectance as well as direct and diffuse transmittance can be described in the framework of four-flux theory [30–32]. This theory gives analytical equations for the reflectance and transmittance components, but it includes a number of poorly known parameters in addition to the scattering and absorption coefficients, including forward scattering ratios, average path-length parameters, and interface reflectance for diffuse light [32]. Inverting the equations to obtain parameter values from experimental data is very hard, and the only option would be to apply advanced fitting methods such as the spectrally projected gradient method that has been employed for a related problem [33].

Two-flux models [31] offer a simpler, although approximate, description of the optics of materials exhibiting diffuse light scattering. The conditions for the applicability of these models have been studied in detail [34,35]. Recent work by Levinson et al. [36] has shown that a two-flux model can be used to approximately describe the total transmittance and reflectance even in cases when there are significant specular components. Apart from interface reflectance, which can be estimated, the model parameters are the phenomenological backscattering and absorption coefficients, *S* and *K*, respectively, of the sample. Methods to obtain these coefficients from experimental data have been suggested [36]. In our present case, it is possible to simplify the treatment because there is information on both specular and diffuse components and, as detailed below, we obtain the extinction coefficient and the interface reflectance for collimated light from the direct transmittance and specular reflectance using basic relations from four-flux theory. This information is then combined with a two-flux model of the total reflectance to obtain *S* and *K* via a modification of the earlier proposed method [36].

3.1. Four-flux theory

The geometry of the SPD is taken to be that of a multilayer stack with the polymer layer incorporating the polarizable particles in the middle and surrounded by two transparent conducting films each backed by a glass substrate. If the refractive indices of the various components are close to each other one can neglect all interface reflections except those at the glass/air interfaces. This approximation is necessary since the optical properties of the transparent conductor (ITO) films, positioned between the glass substrates and the active polymer layer, are not known. The four-flux theory can then be used to provide simple expressions for the direct transmittance and the specular reflectance [30]. When the values of the interface reflectances are small, as in the present case, we neglect multiple reflections and obtain

$$T_{dir} = (1-R_c)^2 e^{-E\delta}, \tag{1}$$

$$R_{spec} = R_c + R_c(1-R_c)^2 e^{-2E\delta}, \tag{2}$$

where R_c is the specular reflectance at the external surfaces, which for most glass and polymer materials would be close to 0.04 and correspond to a refractive index of about 1.5. It is possible to solve these equations in order to obtain the extinction coefficient and R_c from the measurements.

In order to determine both scattering and absorption coefficients, the diffuse components of the reflectance and transmittance have to be considered. The four-flux expressions for the diffuse parts are too complicated to be inverted, though, and contain too many free parameters. Instead we resort to the two-flux theory, as explained next.

3.2. Two-flux theory

Approximate relations for the total transmittance and reflectance can be obtained from the two-flux model as shown recently [36]. It was then assumed that the diffuse light is semi-isotropic and that the diffuse light and the collimated light travel with approximately equal path-lengths through the sample. The case of collimated illumination was treated by the Saunderson approximation [37]. The SPD exhibits a combination of diffuse and collimated light, however, which makes it complicated to estimate the interface reflectances of the model. It should be noted too that no simple relation exists between the extinction and the phenomenological scattering and absorption coefficients.

Our analysis neglects the reflectance at the glass/ITO/polymer interfaces, and hence the SPD is modeled as a simple slab, with thickness d, of an inhomogeneous material surrounded by air. We first consider the Kubelka–Munk approximation for the reflectance and transmittance, denoted R_{KM} and T_{KM}, respectively. The fundamental two-flux equation for the total reflectance of a layer on a substrate (called "background") was derived by Kubelka [38] and is given by

$$R_{KM} = \frac{1-R_g(a-b\coth bSd)}{a-R_g+b\coth bSd}, \tag{3}$$

where R_g is the total reflectance of the background, which in our case is the backside glass/air interface. Eq. (3) was also obtained by Maheu and Gouesbet [31] as a special case of the four-flux theory. The corresponding equation for the total transmittance of a layer on the transparent background can be obtained by putting the background absorption $(1-\tau_d)$ to zero in Eq. (64) of Maheu and Gouesbet [31], i.e.,

$$T_{KM} = \frac{b(1-R_g)}{(a-R_g)\sinh bSd+b\cosh bSd}, \tag{4}$$

which reduces to the equation of Kubelka [38] when $R_g=0$. The parameters a and b that occur in Eqs. (3) and (4) are given in terms of the phenomenological backscattering and absorption coefficients by

$$a = 1+\frac{K}{S}, \tag{5}$$

$$b = \left(a^2-1\right)^{1/2}. \tag{6}$$

This approximation neglects the front surface reflection, and to take it into account we use Saunderson's procedure [37] for the reflectance and obtain

$$R = R_c+\frac{(1-R_c)(1-R_j)R_{KM}}{1-R_jR_{KM}}, \tag{7}$$

where R_c is the reflectance of collimated light incident at the front air/glass interface, as before, and R_j denotes the reflectance of partially diffuse light from within the inhomogeneous material and impinging onto the front glass/air interface. For the transmittance we apply an analogous correction procedure, which gives [39]

$$T = \frac{(1-R_c)T_{KM}}{1-R_jR_{KM}}. \tag{8}$$

Approximations to R_j and R_g are described next. These parameters signify the partly diffuse reflectance at the front and back interface, respectively, to the radiation coming from inside the film. Collimated radiation would exhibit a reflectance equal to R_c, while totally diffuse radiation would have a higher reflectance, denoted R_d, mainly because of total internal reflection at high incidence angles [40]. In order to interpolate between these limiting cases we need to estimate the fraction of diffuse light close to the interfaces of the film. This can be done from measurements of the total and specular reflectance, as well as the total and direct transmittance, by the methods developed in Section 2.6 in the work by Levinson et al. [36]. The intensity of light propagating toward the back interface is denoted $i(z)$, and $j(z)$ represents the intensity of light propagating in the other direction. We take the z-coordinate to be zero at the back interface and d at the front interface. The subscript c on $i(z)$ and $j(z)$ signifies the collimated light intensities. The diffuse light fractions in the film close to the back interface (q_0) and close to the front interface (q_d) are defined as [38]

$$q_0 = 1-(i_c(0)/i(0)), \tag{9}$$

$$q_d = 1-(j_c(d)/j(d)). \tag{10}$$

Relations for the intensities $i_c(0)$, $j_c(d)$, $i(0)$ and $j(d)$ in terms of measurable quantities have been given by Levinson et al. [36]. We express these relations by use of the interface reflectances R_c and R_d, and insert them into Eqs. (9) and (10). This gives

$$q_0 = 1-\frac{T_{dir}[1-((1-q_0)R_c+q_0R_d)]}{T_{tot}(1-R_c)}, \tag{11}$$

$$q_d = 1-\frac{(R_{spec}-R_c)[1-((1-q_d)R_c+q_dR_d)]}{(R_{tot}-R_c)(1-R_c)}. \tag{12}$$

These equations can now be solved in order to obtain q_0 and q_d, the result being

$$q_0 = \frac{(T_{tot}-T_{dir})(1-R_c)}{T_{tot}(1-R_c)-T_{dir}(R_d-R_c)}, \tag{13}$$

$$q_d = \frac{(R_{tot}-R_{spec})(1-R_c)}{R_{tot}(1-R_c)-R_{spec}(R_d-R_c)+R_cR_d-R_c}. \tag{14}$$

The calculations then proceed as follows: (i) The effective refractive index of the film is computed from R_c, as obtained from Eqs. (1) and (2), by inverting the Fresnel relation at normal incidence, $R_c=[(n-1)/(n+1)]^2$, (ii) the diffuse interface reflectance R_d is computed from expressions given by Ryde [41] and Giovanelli [40] and obtained by averaging the Fresnel reflection coefficients over all angles of incidence, (iii) the fractions of diffuse light close to the interfaces of the film are obtained from Eqs. (13) and (14), and (iv) the interface reflectance values R_j and R_g are derived by averaging the specular and diffuse interface reflectance over the diffuse light fractions according to

$$R_{j,g} = (1-q_{d,0})R_c+q_{d,0}R_d, \tag{15}$$

where R_j and R_g are obtained from q_d and q_0, respectively. Subsequently values of S and K are obtained by fitting Eqs. (3)–(8) to measured data.

4. Experimental results

Fig. 3 illustrates the relationship between applied voltage in the $0<U<100$ V range, direct transmittance at $\lambda=600$ nm, and electrical current for the SPD. The highest transmittance, with $T_{dir}\approx 32\%$, was reached for a maximum peak current of $\sim$950 μA obtained at $U=100$ V.

Fig. 4 shows spectral direct and diffuse transmittance (panel a) and specular and diffuse reflectance (panel b) at $350<\lambda<2500$ nm for the SPD operated at zero voltage and at $U=100$ V. The value of T_{dir} drops sharply at $\lambda<1000$ nm when no voltage is applied and attains a distinct minimum at $\lambda\approx 700$ nm. The luminous transmittance—an average over the sensitivity of the eye, which is confined to $400<\lambda<700$ nm and peaked at $\lambda\approx 550$ nm—goes from $\sim$5 to $\sim$35% when the voltage is turned on. The optical modulation is insignificant in the

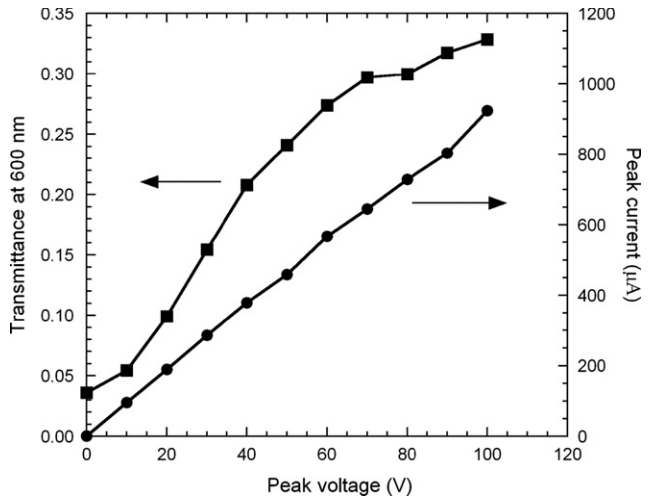

Fig. 3. Electrical current and direct optical transmittance at $\lambda = 600$ nm as a function of applied voltage for an SPD.

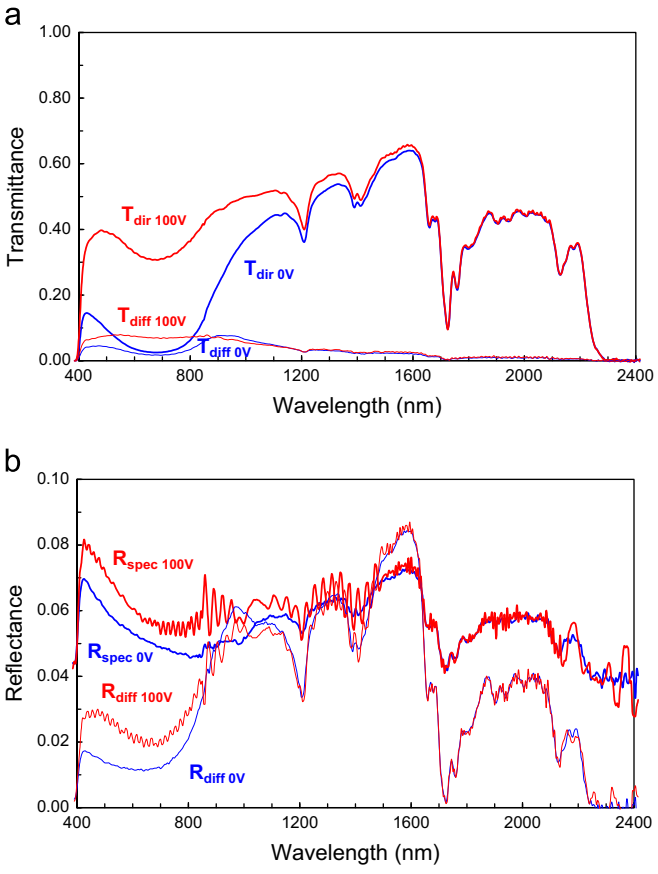

Fig. 4. Spectral direct and diffuse transmittance (panel a) and specular and diffuse reflectance (panel b) for the SPD at zero voltage ("off" state) and at $U = 100$ V ("on" state). The oscillations in the reflectance data between 900 and 1300 nm in wavelength for $U = 100$ V may be caused by optical interference.

infrared for $\lambda > 1000$ nm, and hence the modulation of the solar transmittance—lying in the $300 < \lambda < 3000$ nm interval—is considerably smaller than the modulation of visible light. The magnitude of T_{diff} remains below 10% irrespectively of the wavelength and is large enough to be perceived as haze. The magnitude of R_{spec} lies at 6–8% for luminous radiation

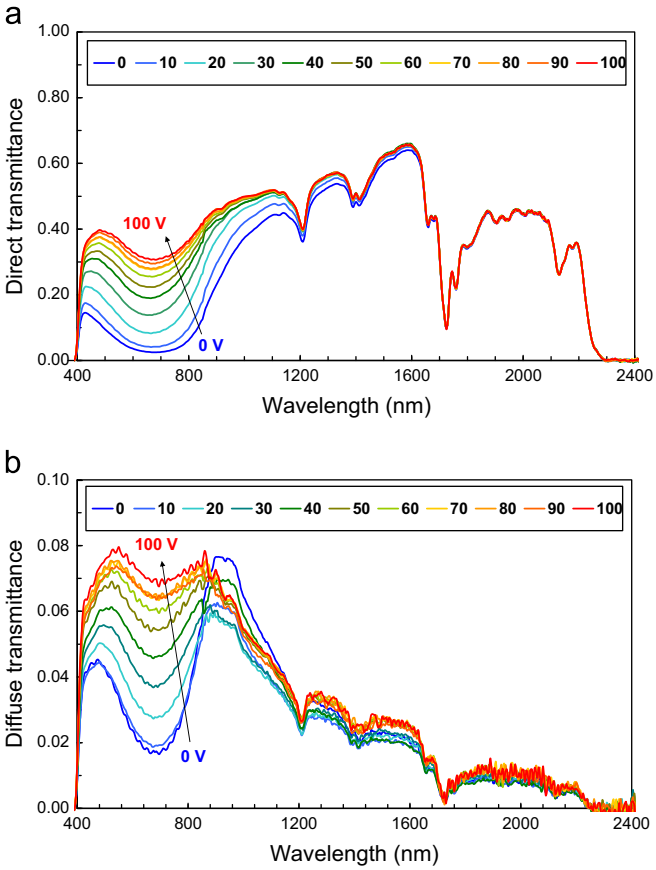

Fig. 5. Spectral direct (panel a) and diffuse (panel b) transmittance for the SPD at applied voltages from zero to100 V, as indicated by the arrows and in the inset. Data for zero voltage and $U = 100$ V were also shown in Fig. 4.

irrespectively of the voltage; the corresponding value of R_{diff} is 2–3%.

The spectral transmittance data are further elucidated in Fig. 5, which shows T_{dir} and T_{diff} for 10 values of applied peak voltage in the $0 < U < 100$ V range. It is evident that the transmittance can be varied monotonically by changing the voltage.

The transmittance modulation is almost entirely confined to the luminous wavelength range, and it is of interest to quantify the luminous and solar transmittance by averaging the spectral transmittance according to

$$T_{tot(diff)-\mathrm{lum,sol}} = \int d\lambda \varphi_{\mathrm{lum,sol}}(\lambda) T_{tot(diff)}(\lambda) / \int d\lambda \varphi_{\mathrm{lum,sol}}(\lambda), \qquad (16)$$

where φ_{lum} is the sensitivity of the light-adapted human eye [42] and φ_{sol} is solar irradiance for air mass 1.5 (the sun at 37° above the horizon) [43]. Fig. 6 shows the wavelength integrated total and diffuse transmittance as a function of voltage and indicates that the luminous total transmittance can be varied in a moderately wide range between 7% and 40%. The solar total transmittance variation is significantly smaller, lying between 22% and 43%, since the SPD does not exhibit any voltage-dependent modulation of the near-infrared transmittance. The solar and luminous values of the diffuse transmittance are both of the order of 3–5%.

Fig. 7 shows T_{tot} at U being zero, 50 V, and 100 V for five values of the incidence angle. The transmittance drops monotonically as θ goes up with the effect being most pronounced for the transparent state. This is as expected since the optical path-

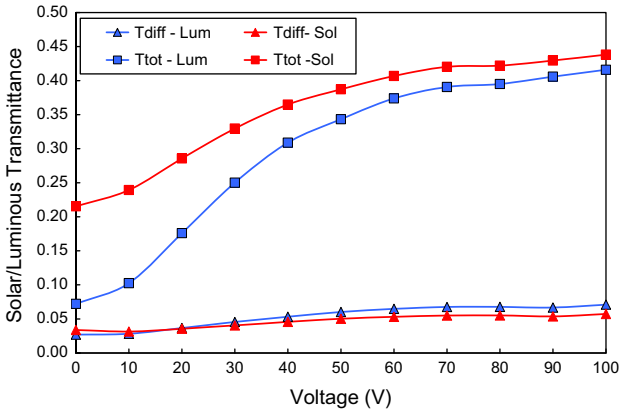

Fig. 6. Solar and luminous total and diffuse transmittance as a function of applied voltage for the SPD. Data were obtained from integrating the spectral information in Fig. 5 over the luminous and solar wavelength ranges, as described in the text.

length through the SPD is enlarged at increasing θ. It is also observed that the voltage-dependent modulation of the transmittance becomes smaller as the incidence angle increases.

5. Determination of absorption and backscattering coefficients

The geometry of the SPD is approximated as a stack with the polymer layer incorporating the polarizable particles in the middle surrounded by two glass substrates. If the refractive indices of the various components are close to each other one can neglect all interface reflections except those at the glass/air interfaces, as discussed above. We now proceed to determine the phenomenological absorption and backscattering coefficients of the particulate layer.

Fig. 8(a) shows extinction coefficients of the SPD, as calculated from Eqs. (1) and (2), for 0 V and for $U=100$ V. The data display a pronounced peak at $\lambda \approx 700$ nm, particularly with the device in its "off" state, which clearly is consistent with the empirical results in Figs. 5–7. The extinction peaks at $\lambda > 1200$ nm are observed irrespectively of applied voltage and are also consistent with the data in the same figures. These peaks are probably due to absorption in the polymer matrix surrounding the active polyiodide particles. Fig. 8(b) reports corresponding results for the interface reflectance, whose values in the luminous wavelength range are significantly higher than 0.04 and correspond to a spectrally dependent refractive index between 1.5 and 1.7. These increased values, exceeding those expected for an air/glass interface, are mainly due to the omission of the reflection at the surfaces of the ITO, which makes the computed R_c an "effective reflectance" with a value higher than 0.04.

The fractions of diffuse light at the interfaces are shown in Fig. 9 for the SPD in "off" and "on" states. It is seen from the values of q_d that light in the SPD layer propagating toward the front interface is mainly diffuse. This is reasonable since it has its origin in backscattering in the SPD layer. On the other hand, light is partially diffuse at the back interface and the diffuse fraction q_0 exhibits a pronounced peak at visible wavelengths.

Spectral interface reflectance data are shown in Fig. 10 for the SPD in "off" and "on" states. Light close to the front interface is mainly diffuse, which leads to a value of R_f of the order of 0.6–0.7. At the bottom interface, the light has a significant diffuse component in the visible wavelength range leading to large interface reflectance. However, the light is mainly collimated for $\lambda > 1200$ nm and then R_g approaches R_c.

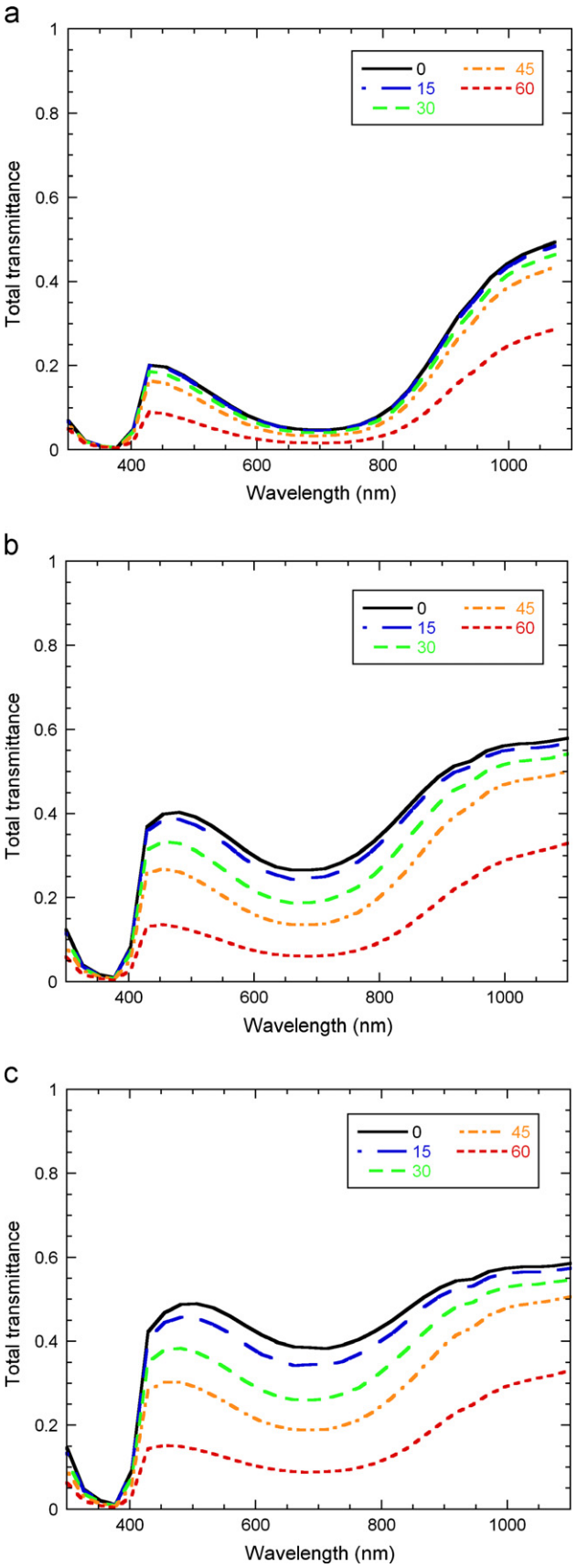

Fig. 7. Spectral total transmittance for the SPD at zero voltage ("off" state) (panel a), for $U=50$ V (panel b) and for $U=100$ V ("on" state) (panel c). Data are given for different incidence angles (given in degrees), as shown in the insets.

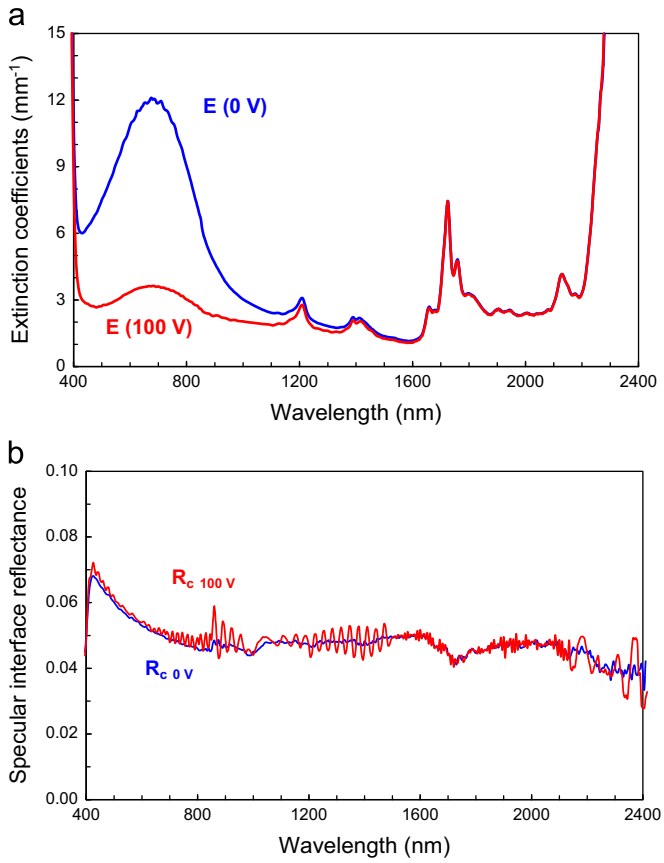

Fig. 8. Spectral extinction coefficient E (panel a) and interface reflectance R_c (panel b) for the SPD at zero voltage ("off" state) and for $U=100$ V ("on" state).

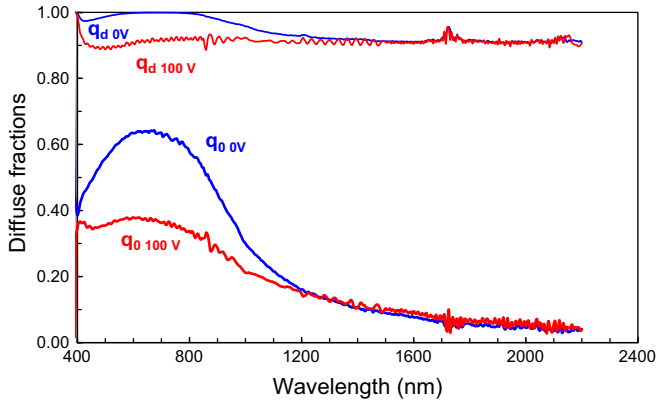

Fig. 9. Diffuse light fractions at the front (q_d, upper curves) and back q_0 (lower curves) interfaces for light exiting the SPD at zero voltage ("off" state) and for $U=100$ V ("on" state).

The phenomenological scattering and absorption coefficients can now be obtained by numerical inversion of Eqs. (3)–(8). The values of S and K obtained from the best fits, for both "off" and "on" states, are plotted in Fig. 11. The scattering coefficient for visible light is seen to be very low when particles (or dipoles) are aligned in the applied field and high when dipole orientation is random. The absorption of visible light is much larger in the absence of an applied voltage, which is as expected. The absorption exhibits a pronounced peak at $\lambda \approx 650$ nm in both states. A peak for mid-luminous wavelengths is characteristic for the optical properties of polyiodide materials [24]. The sharp peaks in the near-infrared are probably related to absorption in the polymer matrix rather than in the particles, as mentioned above.

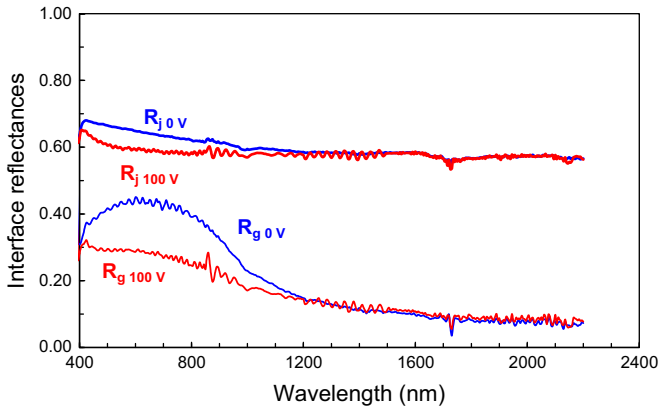

Fig. 10. Interface total reflectance R_j (upper curves) and R_g (lower curves) for light exiting the SPD at zero voltage ("off" state) and for $U=100$ V ("on" state).

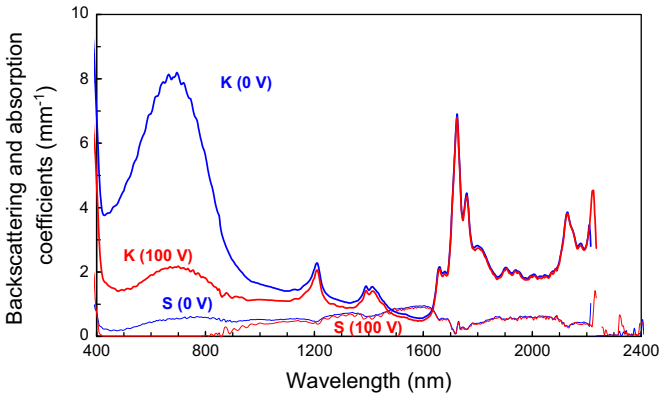

Fig. 11. Scattering S and absorption K coefficients for the SPD at zero voltage ("off" state) and for $U=100$ V ("on" state).

Our use of the two-flux theory rests on several approximations, and therefore it is important to check its consistency with the measured data on R_{tot} and T_{tot}. This also serves as a weak [36] consistency check on our values of S and K. Fig. 12 shows a comparison of the measured data with two-flux computations for the total reflectance with the SPD in fully transparent and dark states. Very good agreement is indeed observed, the only discrepancy being a slight underestimation of the reflectance for the transparent state with regard to the luminous wavelength range.

6. Conclusions

We used spectral optical measurements of total and diffuse transmittance and reflectance to characterize a suspended particle device, thereby expanding previous work on electrical characterization of such devices [15,16]. Optical transmission could be modulated within widely separated limits for luminous light, whereas the near-infrared modulation was almost nil. The samples showed some diffuse light scattering (haze), which can be a disadvantage for applications. Scattering and absorption coefficients were computed from experimental data using a modification of the model of Levinson et al. [36]. This information will make it possible to optimize and design devices by model computations, starting from basic parameters that describe the optical properties of the particulate material. The diffuse transmittance and reflectance in the visible spectral range for the present SPDs shows that there is room for improvement concerning their uses in smart windows technology.

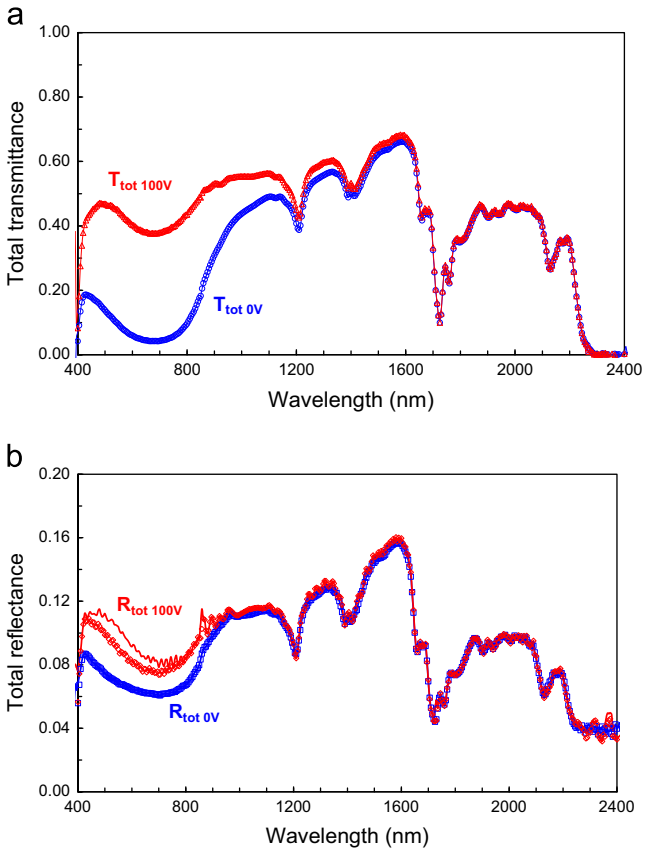

Fig. 12. Total transmittance (panel a) and reflectance (panel b) from experiments (curves) and from two-flux computations (symbols) using the parameters provided in Fig. 8(b) and Figs. 9–11. Data are given for the SPD at zero voltage ("off" state) and for $U=100$ V ("on" state).

Acknowledgment

We are grateful to CIDETEC for providing the SPD window sample. Universidad Carlos III is thanked for supporting DB's research in Sweden. This work was supported in part by the Comunidad de Madrid (FACTOTEM2-CM, S2009/ESP-1781). Work at Uppsala University was financially supported by the Swedish Research Council (VR).

References

[1] C.M. Lampert, C.G. Granqvist (Eds.), Large-Area Chromogenics: Materials and Devices for Transmittance Control, SPIE Optical Engineering Press, Bellingham, WA, USA, 1990.
[2] C.M. Lampert, Smart switchable glazing for solar energy and daylight control, Solar Energy Materials and Solar Cells 52 (1998) 207–221.
[3] G.B. Smith, C.G. Granqvist, Green Nanotechnology: Solutions for Sustainability and Energy in the Built Environment, CRC Press, Boca Raton, FL, USA, 2010.
[4] B. Richter, D. Goldston, G. Crabtree, L. Glicksman, D. Goldstein, D. Greene, D. Kammen, M. Levine, M. Lubell, M. Savitz, D. Sperling, F. Schlachter, J. Scofield, J. Dawson, How America can look within to achieve energy security and reduce global warming, Reviews of Modern Physics 80 (2008) S1–S107.
[5] D.T. Gillaspie, R.C. Tenent, A.C. Dillon, Metal-oxide films for electrochromic applications: present technology and future directions, Journal of Materials Chemistry 20 (2010) 9585–9592.
[6] C.G. Granqvist, Handbook of Inorganic Electrochromic Materials, Elsevier, Amsterdam, The Netherlands, 1995.
[7] G.A. Niklasson, C.G. Granqvist, Electrochromics for smart windows: thin films of tungsten oxide and nickel oxide, and devices based on these, Journal of Materials Chemistry 17 (2007) 127–156.
[8] C.G. Granqvist, Oxide electrochromics: an introduction to devices and materials, Solar Energy Materials and Solar Cells 99 (2012) 1–13.
[9] J.L. Slack, J.C.W. Locke, S.-W. Song, J. Ona, T.J. Richardson, Metal hydride switchable mirrors: factors influencing dynamic range and stability, Solar Energy Materials and Solar Cells 90 (2006) 485–490.
[10] K. Tajima, Y. Yamada, S. Bao, M. Okada, K. Yoshimura, Optical switching properties of all-solid-state switchable mirror glass based on magnesium-nickel thin film for environmental temperature, Solar Energy Materials and Solar Cells 94 (2010) 227–231.
[11] P.M.S. Monk, R.J. Mortimer, D.R. Rosseinsky, Electrochromism and Electrochromic Devices, Cambridge University Press, Cambridge, UK, 2007.
[12] G. Beni, H.G. Craighead, S. Hackwood, Anisotropic suspension display, Applied Physics Letters 39 (1981) 195–197.
[13] H. Takeuchi, A. Usuki, N. Tatsuda, H. Tanaka, A. Okada, K. Tajima, Suspended particle display using novel complexes, Materials Research Society Symposium Proceedings 424 (1997) 317–322.
[14] B.-S. Yu, E.-S. Kim, Y.-W. Lee, Developments in suspended particle devices (SPD), Proceedings of the Society for Photo-Optical Instrumentation Engineers 3138 (1997) 217–225.
[15] R. Vergaz, J.M.S. Pena, D. Barrios, I. Pérez, J.C. Torres, Electrooptical behaviour and control of a suspended particle device, Opto-Electronics Review 15 (2007) 154–158.
[16] R. Vergaz, J.-M. Sánchez-Pena, D. Barrios, C. Vásquez, P. Contreras-Lallana, Modelling and electro-optical testing of suspended particle devices, Solar Energy Materials and Solar Cells 92 (2008) 1483–1487.
[17] D. Cupelli, F.P. Nicoletta, S. Manfredi, G. De Filpo, G. Chidichimo, Electrically switchable chromogenic materials for external glazing, Solar Energy Materials and Solar Cells 93 (2009) 329–333.
[18] D. Cupelli, F.P. Nicoletta, S. Manfredi, M. Vivacqua, P. Formoso, G. De Filpo, G. Chidichimo, Self-adjusting smart windows based on polymer-dispersed liquid crystals, Solar Energy Materials and Solar Cells 93 (2009) 2008–2012.
[19] J.P. Ziegler, Status of reversible electrodeposition electrochromic devices, Solar Energy Materials and Solar Cells 56 (1999) 477–493.
[20] B. Laik, C. Carrière, J.-M. Tarascon, Reversible electrochromic system based on aqueous solution containing silver, Electrochimica Acta 46 (2001) 2203–2209.
[21] A.M. Marks, Electrooptical characteristics of dipole suspensions, Applied Optics 8 (1969) 1397–1412.
[22] B. Kahr, J. Freudenthal, S. Phillips, W. Kaminsky, Herapathite, Science 324 (2009) 1407.
[23] K.M. Knowles, Herapathite: The first man-made polarizer, Philosophical Magazine Letters 89 (2009) 745–755.
[24] L. Liang, P. Rulis, B. Kahr, W.Y. Ching, Theoretical study of the large linear dichroism of herapathite, Physical Review B 80 (2009) 235132/1–235132/5.
[25] B. Fanning, R.L. Saxe, S.M. Slovak R.I. Thompson, Polyhalide particles and light valves comprising same, US Patent 6517746 (2003).
[26] S. Charapani, S.M. Slovak, R.L. Saxe, B. Fanning, SPD films and light valves comprising same, US Patent 6416827 (2002).
[27] A. Roos, Use of an integrating sphere in solar energy research, Solar Energy Materials and Solar Cells 30 (1993) 77–94.
[28] A. Roos, Materials performance and systems performance, in: M. Köhl, B. Carlsson, G. Jorgensen, A.W. Czanderna (Eds.), Performance and Durability Assessment: Optical Materials for Solar Energy Systems, Elsevier, Amsterdam, The Netherlands, 2004.
[29] P. Nostell, A. Roos, D. Rönnow, Single-beam integrating sphere spectrophotometer for reflectance and transmittance measurements versus angle of incidence in the solar wavelength range on diffuse and specular samples, Review of Scientific Instruments 70 (1999) 2481–2494.
[30] B. Maheu, J.N. Letoulouzan, G. Gouesbet, Four-flux models to solve the scattering transfer equation in terms of Lorenz–Mie parameters, Applied Optics 23 (1984) 3353–3362.
[31] B. Maheu, G. Gouesbet, Four-flux models to solve the scattering transfer equation: special cases, Applied Optics 25 (1986) 1122–1128.
[32] W.E. Vargas, Generalized four-flux radiative transfer model, Applied Optics 37 (1998) 2615–2623.
[33] F. Curiel, W.E. Vargas, R.G. Barrera, Visible spectral dependence of the scattering and absorption coefficients of pigmented coatings from inversion of diffuse reflectance spectra, Applied Optics 41 (2002) 5969–5978.
[34] W.E. Vargas, G.A. Niklasson, Applicability conditions of the Kubelka–Munk theory, Applied Optics 36 (1997) 5580–5586.
[35] W.E. Vargas, Two-flux radiative transfer model under nonisotropic propagating diffuse radiation, Applied Optics 38 (1999) 1077–1085.
[36] R. Levinson, P. Berdahl, H. Akbari, Solar spectral optical properties of pigments—Part I: model for deriving scattering and absorption coefficients from transmittance and reflectance measurements, Solar Energy Materials and Solar Cells 89 (2005) 319–349.
[37] J.L. Saunderson, Calculation of the color of pigmented plastics, Journal of the Optical Society of America 32 (1942) 727–736.
[38] P. Kubelka, New contributions to the optics of intensely light-scattering materials. Part I, Journal of the Optical Society of America 38 (1948) 448–457.
[39] G. Kortum, Reflectance Spectroscopy: Principles, Methods, Applications, Springer, Berlin, 1969.
[40] R.G. Giovanelli, A note on the coefficient of reflection for internally incident diffuse light, Journal of Modern Optics 3 (1956) 127–130.
[41] J.W. Ryde, The scattering of light by turbid media—Part 1, Proceedings of the Royal Society of London Series A 131 (1931) 451–464.
[42] G. Wyszecki, W.S. Stiles, Color Science: Concepts and Methods, Quantitative Data and Formulae, 2nd ed., Wiley, New York, USA, 2000.
[43] ASTM G173-03, Standard Tables of Reference Solar Spectral Irradiances: Direct Normal and Hemispherical on a 37° Tilted Surface, Annual Book of ASTM Standards, American Society for Testing and Materials, Philadelphia, PA, USA, 2008, Vol. 14.04; 〈http://rredc.nrel.gov/solar/spectra/am1.5〉.